Fullerenes, Nanotubes, and Carbon Nanostructures, 18: 474–486, 2010

ISSN: 1536-383X print / 1536-4046 online
DOI: 10.1080/1536383X.2010.487785

Taylor & Francis
Taylor & Francis Group

Thermal Conduction in Suspended Graphene Layers

A. A. BALANDIN, S. GHOSH, D. L. NIKA AND E. P. POKATILOV

Nano-Device Laboratory, Department of Electrical Engineering and Materials Science and Engineering Program, University of California – Riverside, Riverside, California

We review the results of our experimental and theoretical investigation of heat conduction in suspended graphene layers. Through direct measurements using a noncontact optical technique, we established that the thermal conductivity of the suspended graphene flakes is extremely high, and exceeds that of diamond and carbon nanotubes. By invoking Klemens' theoretical model, we explained the physical mechanisms behind such unusual thermal conduction in two-dimensional graphene layers. Our detailed theory, which includes the phonon-mode dependent Gruneisen parameter and takes into account phonon scattering on graphene edges and point defects, gives results in excellent agreement with the measurements. Superior thermal properties of graphene are beneficial for all proposed graphene device applications.

Keywords Graphene, Thermal conductivity, Carbon materials, Phonons

Introduction

In recent years, there has been a fast growth in interest of the scientific and engineering research communities to the thermal conductivity of materials. This is explained by both the practical needs, example, heat removal is now a crucial issue for the continuing progress in electronic industry, as well as by fundamental science, that is, material's ability to conduct heat is rooted deeply in its atomic structure and the knowledge of thermal conductivity can shed light on many other materials' properties. Materials with very high or very low thermal conductivities attract particular attention due to possible applications in either heat removal, example, thermal management of electronic circuits or thermal insulation. It was recently discovered experimentally that graphene (1,2) reveals an extremely high thermal conductivity (3,4). The measurements by Balandin et al. (3,4) were performed with a noncontact optical technique, where the local temperature rise due to the laser heating was determined through the independently measured temperature coefficients of the peaks in graphene Raman spectrum (5,6). It was found that the near room-temperature (RT) thermal conductivity of partially suspended single-layer graphene is in the range K $\sim$ 3000–5300 W/mK depending on the graphene flake size. These experiments stimulated theoretical work on the subject. Nika et al. (7) performed detail numerical study of the thermal conductivity of graphene using the phonon dispersion obtained from the valence-force field (VFF) method and treating the three-phonon Umklapp scattering directly considering all phonon relaxation channels allowed in graphene's 2D Brillouin zone (BZ) (7). Jiang et al. (8) calculated the thermal conductance of graphene in the pure ballistic limit obtaining a very high value,

Address correspondence to A. A. Balandin, Nano-Device Laboratory, Department of Electrical Engineering and Materials Science, Engineering Program, University of California–Riverside, Riverside, CA 92521. E-mail: balandin@ee.ucr.edu

which is expected for the ballistic regime when no scattering is present. Lan et al. (9) determined the thermal conductivity of graphene nanoribbons combining the tight-binding approach and the phonon nonequilibrium Green's function method. The authors found a thermal conductivity K = 3410 W/mK (9), which is clearly above the bulk graphite limit of 2000 W/mK and in agreement with the first experiments (3,4).

In this paper we review our experimental and theoretical results pertinent to thermal conduction in suspended graphene layers. The term "suspended" is used to emphasize that the experimental results were achieved for partially suspended graphene flakes not covered by any cap or insulating layer, which might have reduced the heat conduction through graphene. In the theoretical sense, the term suspended indicates that the theory does not include any graphene–substrate interaction, example, the derivation is performed for graphene in free space.

The rest of the paper is organized as follows. Section 2 describes the experimental procedures for measuring the thermal conductivity of graphene. Section 3 outlines the theory of the thermal conductivity. In section 4, we propose a simplified model for the thermal conductivity of graphene, which allows one to see the physical reasons behind higher thermal conductivity of graphene compared to that of basal planes of bulk graphite. The model can be used for quick estimates of the thermal conductivity in graphene flakes of different sizes. The extremely high thermal conductivity of graphene comes in contrast to that of some other carbon materials such as diamond-like carbon or amorphous carbon. The comparison of the heat conduction in graphene with that in other carbon allotropes and derivatives is given in the section 5.

Experimental Study of Heat Conduction in Suspended Graphene

In order to measure the thermal conductivity of suspended graphene layers, we developed our own noncontact optical approach. We took advantage of the fact that graphene has distinctive signatures in Raman spectra with clear *G* peak and *2D* band (10–13). Moreover, we also found that the *G* peak of graphene's Raman spectra exhibits strong temperature dependence (5,6). The latter means that the shift in the position of *G* peak in response to the laser heating can be used for measuring the local temperature rise. The correlation between the temperature rise and amount of power dissipated in graphene, for the sample with given geometry and proper heat sinks, can give the value of the thermal conductivity K (see the schematic of the experiment in Figure 1). Even a small amount of power dissipated in graphene can be sufficient for inducing a measurable shift in the *G* peak position due to the extremely small thickness of the material–one atomic layer. The suspended portion of graphene served several essential functions for (i) accurately determining the amount of power absorbed by graphene through the calibration procedure, (ii) forming two-dimensional in-plane heat front propagating toward the heat sinks, (iii) and reducing the thermal coupling to the substrate through the increased micro- and nanoscale corrugations.

The first step in the measurements was determining the temperature coefficient χ_G for the *G* peak. To accomplish this task, the laser excitation power was kept at a minimal level and the temperature of the graphene flake was changed externally through the hot–cold cell (5,6). After the change in the temperature ΔT has been correlated with the change in the $\Delta\omega$ peak position, the micro-Raman spectrometer can be used as a thermometer. During the measurement of the thermal conductivity the excitation power is intentionally increased to induce the local heating. The local temperature rise is determined through the expression $\Delta T = \Delta\omega_G/\chi_G$. It is important to mention that the measurement technique is steady-state. Each data point in the thermal conductivity measurement, that is, recording the *G* peak position as a function of the excitation power, takes sufficient time (several minutes) for achieving the steady-state. The energy

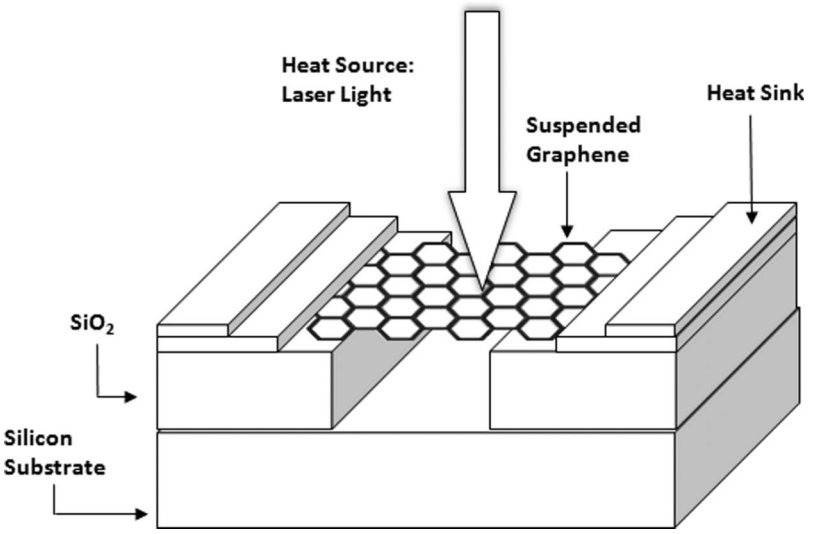

Figure 1. Schematic of the experiments for direct measurements of the thermal conductivity of the suspended graphene layers attached to heat sinks.

deposited by the laser light to the electron gas in graphene is being transferred to phonons very fast. The time constant for the energy transfer from the electrons to acoustic phonons in graphene is on the order of several pico-seconds (14–16). Thus, for the large graphene flakes utilized in our experiments (tens of microns), the changes in the induced hot spot due to the finite thermalization time are small and can be neglected. From the other side, our measurement time was small compared to hours, which are required in order to induce damage or surface modification in graphene by the laser light (17).

The long graphene flakes for these measurements were produced using the standard technique of mechanical exfoliation of bulk Kish and highly oriented pyrolytic graphite (HOPG) (1,2). The trenches were fabricated using the reactive ion etching. The width of these trenches ranged from 1 μm to 5 μm with the nominal depth of 300 nm. In the first set of measurements we selected graphene flakes of approximately rectangular shape connected to large graphitic pieces, which acted as heat sinks. The rectangular shape was selected in order to use a simple data extraction procedure based on the one-dimensional heat diffusion equation. These graphitic pieces were at a distance of few micrometers from the trench edges to ensure that the transport is at least partially diffusive and the phonon mean free path (MFP) is not limited just by the length of the flake. In the later measurements we utilized well-defined massive metal heat sinks and elaborate procedure for the thermal conductivity extraction based on the numerical solution of the heat diffusion equation. The single layer graphene flakes were selected using the micro Raman spectroscopy by checking the intensity ratio of *G* and *2D* peaks and by *2D* band deconvolution (10–13). The combination of these two Raman techniques with the atomic force microscopy (AFM) and scanning electron microscopy (SEM) allowed us to verify the number of atomic planes and flake uniformity with a high degree of accuracy.

The challenge in the measurement of the thermal conductivity with the described optical technique is in accurate determining of the power absorbed in graphene. Only fraction P_G of the laser light focused on graphene flake will actually be dissipated in the graphene. Most of the light will be reflected back after the light travels through the flake to the trench bottom and

reflected back. The power, which is measured by the detector placed at the position of the flake, is the total power P_D, part of which goes into the graphene flake after two transmissions (incident pass and reflected pass), and the rest is lost in the silicon wafer P_{Si}. The fraction of the power absorbed by graphene is 2.3% per layer for light wavelength $\lambda > 500$ nm. Our measurements were performed at smaller wavelength ($\lambda = 488$ nm) where the absorption is enhanced (18,19). Thus, it was important to determine the absorbed power in the specific conditions of our experiment. The power P_G has been measured through the calibration procedure with the bulk graphite serving as a reference. It is based on comparison of the experimentally determined integrated Raman intensity for G peak from the single layer graphene and bulk graphite (4). With the calibration procedure in place for converting P_D to P_G, the measurement of the thermal conductivity of suspended graphene reduces to measuring the Raman shift $\Delta\omega_G$ as the function of the heating power P_D determined by the detector. The measured slope $\Delta\omega/\Delta P_D$, ratio of the integrated intensities ζ and the temperature coefficient χ_G give the value of the thermal conductivity of graphene. The thermal data extraction was accomplished initially with the simple one-dimensional model and later improved by utilizing the numeric solution of the heat diffusion equation for a given flake shape. It has been found that the near room temperature (RT) thermal conductivity of the single layer suspended graphene is in the range from ~3000 W/mK to 5300 W/mK depending on the size of the graphene flakes. The values obtained for graphene are very high as compared with other carbon materials (21–26). The discussion of the wide range of the thermal conductivities for different type of carbon materials is given in the section IV. In section III and IV we explain the origin of the thermal conductivity dependence on the graphene layer size.

Theory of Heat Conduction in Graphene

In this section we outline the theory of heat conduction in graphene. The heat flux along a graphene atomic plane can be calculated according to the expression (27)

$$\vec{W} = \sum_{s,\vec{q}} \vec{v}(s,\vec{q})\hbar\omega_s(\vec{q})N(\vec{q},\omega_s(\vec{q})) = \sum_{s,\vec{q}} \vec{v}(s,\vec{q})\hbar\omega_s(\vec{q})n(\vec{q},\omega_s) \tag{1}$$

where $\vec{v}(s,\vec{q})\hbar\omega_s(\vec{q})$ is the energy carried by one phonon, $\vec{v}(s,\vec{q}) = d\omega_s/dq$ is the phonon group velocity, and $N(\omega,\vec{q}) = N_0(\omega,\vec{q}) + n(\omega,\vec{q})$ is the number of phonons in the flux. Here N_0 is the Bose-Einstein distribution function and $n = -\tau_{tot}(\vec{v}\nabla T)\partial N_0/\partial T$ is the nonequilibrium part of the phonon distribution function N, where τ_{tot} the total phonon relaxation time and T is the absolute temperature.

Comparing the microscopic expression

$$\vec{W} = -\sum_{\beta} (\nabla T)_\beta \sum_{s,\vec{q}} \tau_{tot}(s,\vec{q})v_\beta(s,\vec{q})\frac{\partial N_0(\omega_s)}{\partial T}\vec{v}(s,\vec{q})\hbar\omega_s(\vec{q}) \tag{2}$$

with the macroscopic definition of the thermal conductivity

$$W_\alpha = -\kappa_{\alpha\beta}(\nabla T)_\beta h L_x L_y \tag{3}$$

we obtain the following expression for the thermal conductivity tensor

$$\kappa_{\alpha\beta} = \frac{1}{hL_xL_y}\sum_{s,\vec{q}} \tau_{tot}(s,\vec{q})v_\alpha(s,\vec{q})v_\beta(s,\vec{q})\frac{\partial N_0(\omega_s)}{\partial T}\hbar\omega_s(\vec{q}) \tag{4}$$

Here $L_x = d$ is the sample width (graphene flake width), L_y is the sample length and $h = 0.35$ nm is the thickness of graphene. The diagonal element of the thermal conductivity tensor, which corresponds to the phonon flux along the temperature gradient, is given by

$$\kappa_{\alpha\alpha} = \frac{1}{hL_xL_y}\sum_{s,\vec{q}} \tau_{tot}(s,\vec{q})v^2(s,\vec{q})\cos^2\varphi\frac{\partial N_0(\omega_s)}{\partial T}\hbar\omega_s(\vec{q}) \tag{5}$$

Finally, making a transition from the summation to integration and taking into account the two-dimensional of density of phonon states, we obtain the expression for the scalar thermal conductivity

$$K = \frac{1}{4\pi k_B T^2 h}\sum_s \int_0^{q_{\max}} \{[\hbar\omega_s(q)\frac{d\omega_s(q)}{dq}]^2\tau_{tot}(s,q)\frac{\exp[\hbar\omega_s(q)/kT]}{[\exp[\hbar\omega_s(q)/kT]-1]^2}q\}dq \tag{6}$$

The detailed description of the theoretical formalism for the phonon heat conduction in graphene was recently reported elsewhere (7). Our theoretical approach utilized an original *phase-diagram technique* to account for all three-phonon Umklapp scattering channels allowed by the energy and momentum conservation. We consider two types of the three-phonon Umklapp scattering processes (27–29). The first type is the scattering when a phonon with the wave vector $\vec{q}(\omega)$ absorbs another phonon from the heat flux with the wave vector $\vec{q}'(\omega')$, that is, the phonon leaves the state $\vec{q}$. For this type of scattering processes the momentum and energy conservation laws are written as

$$\begin{aligned} \vec{q} + \vec{q}' &= \vec{b}_i + \vec{q}'' \\ \omega + \omega' &= \omega'' \end{aligned} \tag{7}$$

where $\vec{b}_i, i = 1,2,3$ is one of the vectors of reciprocal lattice. The processes of the second type are those when the phonons $\vec{q}$ of the heat flux decay into two phonons with the wave vectors $\vec{q}'$ and $\vec{q}''$ leaving the state $\vec{q}$, or, alternatively, two phonons $\vec{q}'(\omega')$ and $\vec{q}''(\omega'')$ merge together forming a phonon with the wave vector $\vec{q}(\omega)$, which correspond to the phonon coming to the state $\vec{q}(\omega)$. The conservation laws for this type are given by

$$\begin{aligned} \vec{q} + \vec{b}_i &= \vec{q}' + \vec{q}'', \quad i = 4,5,6 \\ \omega &= \omega' + \omega'' \end{aligned} \tag{8}$$

To find all possible three-phonon processes we used a fine mesh $q_j = (j-1)\Delta q$ $(j = 1, \ldots, 1001)$ with the step $\Delta q = q_{\max}/1000 \approx 0.015\,\text{nm}^{-1}$. For each phonon mode ($q_i$, S), we found all pairs of the phonon modes $(\vec{q}', s')$ and $(\vec{q}'', s'')$ such that the conditions of equations (7–8) are met. The latter can be done with the help of $(\vec{q}')$-space *phase diagrams* technique, which we introduced in Ref. (7).

Using the general expression for a matrix element of the three-phonon interaction (27–29) and taking into account all relevant phonon branches and their dispersion as well as all unit vectors of the reciprocal lattice $\vec{b}_1 \ldots\ldots \vec{b}_6$, directed from the Γ point to the centers of the neighbouring unit cells, we obtain for the Umklapp scattering rates

$$\frac{1}{\tau_U^{(I),(II)}(s,\vec{q})} = \frac{\hbar\gamma_s^2(\vec{q})}{3\pi\rho v_s^2(\vec{q})} \sum_{s's'';\vec{b}_i} \iint \omega_s(\vec{q})\omega'_{s'}(\vec{q}')\omega''_{s''}(\vec{q}'') \times \{N_0[\omega'_{s'}(\vec{q}')] \mp N_0[\omega''_{s''}(\vec{q}'')] + \frac{1}{2} \mp \frac{1}{2}\} \times \delta[\omega_s(\vec{q}) \pm \omega'_{s'}(\vec{q}') - \omega''_{s''}(\vec{q}'')] dq'_l dq'_\perp \tag{9}$$

Here q'_l and $q'_\perp$ are the components of the vector $\vec{q}'$ parallel or perpendicular to the lines defined by equations (7–8); correspondingly, $\gamma_s(\vec{q})$ is the mode-dependent Gruneisen parameter, which is determined for each phonon wave vector and polarization branch and ρ is the surface mass density. In equation (9) the upper signs correspond to the processes of the first type while the lower signs correspond to those of the second type. Integrating along $q_\perp$ we obtain the line integral

$$\frac{1}{\tau_U^{(I),(II)}(s,\vec{q})} = \frac{\hbar\gamma_s^2(\vec{q})\omega_s(\vec{q})}{3\pi\rho v_s^2(\vec{q})} \sum_{s's'';\vec{b}} \int_l \frac{\pm(\omega''_{s''} - \omega_s)\omega''_{s''}}{v_\perp(\omega'_{s'})} (N'_0 \mp N''_0 + \frac{1}{2} \mp \frac{1}{2}) dq'_l \tag{10}$$

The combined scattering rate in both types of the three-phonon Umklapp processes for a phonon in the state $(s,\vec{q})$ is a sum of first and second types of the Umklapp processes. For the small phonon wave vectors (long wave length), $q \to 0$, the Umklapp limited phonon lifetime $\tau_U \to \infty$. For this reason, the calculation of the intrinsic thermal conductivity with only Umklapp scattering is not possible without an arbitrary truncation procedure.

To avoid the unphysical assumptions about the limits of the integration in the thermal conductivity integral, one can include the phonon scattering on boundaries. In the case of graphene, the boundary scattering term correspond to scattering from the rough edges of graphene flakes. No scattering happens from the top and bottom sides of graphene flake since it is only one atomic layer thick and the phonon flux is parallel to the graphene plane. One can evaluate the rough edges scattering using a well-known equation (30)

$$\frac{1}{\tau_B(s,q)} = \frac{v_s(\omega_s)}{L} \frac{1-p}{1+p} \tag{11}$$

Here p is the specularity parameter, which depends on the roughness at the graphene edges and L is the width of the graphene flake. The total phonon relaxation rate is found as a sum of the Umklapp and edge scattering. It is important to understand that the thermal conductivity of the two-dimensional system such as graphene cannot be determined without the restriction on the phonon MFP in the long wave length limit. The phonon scattering on edges restricts the MFP in the formal theory of thermal conductivity. In this sense the thermal conductivity limited by the Umklapp and boundary scattering can be considered as an *intrinsic* property of a graphene flake of a particular size. The extrinsic effects, which reduce the thermal conductivity, such as phonon scattering on defects, impurities and grain boundaries are not included into the consideration.

Lattice Thermal Conductivity of Graphene

The calculation of the thermal conductivity within the formal theory outlined in the previous section is a rather complicated procedure. In this section, we describe a simple model of the thermal conductivity of graphene. This model uses a rather general expression for the thermal conductivity with the two Gruneisen parameters γ_s obtained independently for

each of the heat conducting phonon polarization branches S, and separate phonon velocities and cut-off frequencies for each phonon branch. The model includes the specifics of the phonon dispersion in graphene. The effective parameters γ_s are computed by averaging the phonon mode-dependent $\gamma_s(\vec{q})$ for all relevant phonons (here $\vec{q}$ is the phonon wave vector). The phonon branches, which carry heat, are longitudinal acoustic (*LA*) and transverse acoustic (*TA*). The out-of-plane transverse acoustic phonons (*ZA*) do not make contributions to heat conduction due to their low group velocity and high $\gamma_s(\vec{q})$.

There is a clear difference in the heat transport in basal planes of bulk graphite and in single layer graphene (25,26). In the former, the heat transport is approximately two-dimensional only till some low-bound cut-off frequency ω_C. Below ω_C there appears strong coupling with the cross-plane phonon modes and heat starts to propagate in all directions, which reduces the contributions of these low-energy modes to heat transport along basal planes to negligible values. In bulk graphite there is a physically reasonable reference point for the on-set of the cross-plane coupling, which is the ZO′ phonon branch near ~4 THz observed in the spectrum of bulk graphite. The presence of ZO′ branch and corresponding ω_C allows one to avoid the logarithmic divergence in the Umklapp-limited thermal conductivity integral and calculate it without considering other scattering mechanisms. The physics of heat conduction is principally different in graphene where the phonon transport is pure two-dimensional all the way to zero phonon frequency $\omega(q = 0) = 0$. There is no on-set of the cross-plane heat transport at the long-wavelength limit in the system, which consists of only one atomic plane. This is no ZO′ branch in the phonon dispersion of graphene. Thus, the cut-off frequency for Umklapp processes can not be introduced by analogy with bulk graphite.

Using an expression for the three-phonon Umklapp scattering from Refs. (25,26) but introducing separate life-times for LA and TA phonons, one can write

$$\tau^K_{U,s} = \frac{1}{\gamma_s^2}\frac{M\upsilon_s^2}{k_B T}\frac{\omega_{s,\max}}{\omega^2} \tag{12}$$

where s=*TA*, *LA*, υ_s is the average phonon velocity for a given branch, T is the absolute temperature, k_B is the Boltzmann constant, $\omega_{s,\max}$ is the maximum cut-off frequency for a given branch and M is the mass of an atom. To determine γ_s we averaged $\gamma_s(q)$ obtained from the accurate phonon dispersion calculated using VFF method (7) and *ab initio* theory (31). Substituting $\tau_{tot} = \tau^K_{U,s}$ in Equation (6) one can obtain the following formula for intrinsic thermal conductivity in graphene

$$K_U = \frac{1}{4\pi k_B T^2 h}\sum_{s=TA,LA}\int_{q_{\min}}^{q_{\max}}\{[\hbar\omega_s(q)\frac{d\omega_s(q)}{dq}]^2\tau^K_{U,s}(q)\frac{exp[\hbar\omega_s(q)/kT]}{[exp[\hbar\omega_s(q)/kT]-1]^2}q\}dq \tag{13}$$

The above equation can be used to calculate the thermal conductivity with the actual dependence of the phonon frequency $\omega_s(q)$ and the phonon velocity $d\omega_s(q)/dq$ on the phonon wave number. To simplify the model further one can use the linear dispersion $\omega_s(q) = \upsilon_s q$ and rewrite it as

$$K_U = \frac{\hbar^2}{4\pi k_B T^2 h}\sum_{s=TA,LA}\int_{\omega_{\min}}^{\omega_{\max}}\{\omega^3\tau^K_{U,s}(\omega)\frac{exp[\hbar\omega/kT]}{[exp[\hbar\omega/kT]-1]^2}\}d\omega \tag{14}$$

Substituting equation (12) to equation (13) and performing integration one obtains

$$K_U = \frac{M}{4\pi Th} \sum_{s=TA,LA} \frac{\omega_{s,\max} \upsilon_s^2}{\gamma_s^2} F(\omega_{s,\min}, \omega_{s,\max}) \tag{15}$$

where

$$F(\omega_{s,\min}, \omega_{s,\max}) = \int_{\hbar\omega_{s,\min}/k_BT}^{\hbar\omega_{s,\max}/k_BT} \xi \frac{exp(\xi)}{[exp(\xi)-1]^2} d\xi = [ln\{exp(\xi)-1\} + \frac{\xi}{1-\exp(\xi)} - \xi]|_{\hbar\omega_{s,\min}/k_BT}^{\hbar\omega_{s,\max}/k_BT} \tag{16}$$

In equation (16), $\xi = \hbar\omega/k_BT$, and the upper cut-off frequencies $\omega_{s,\max}$ are defined from the actual phonon dispersion in graphene, calculated using VFF model (7): $\omega_{LA,\max} = 241$ THz, $\omega_{TA,\max} = 108$ THz. The low-bound cut-off frequencies $\omega_{s,\min}$ for each S are determined from the condition that the phonon MFP cannot exceed the physical size L of the flake, that is,

$$\omega_{s,\min} = \frac{\upsilon_s}{\gamma_s} \sqrt{\frac{M\upsilon_s}{k_BT} \frac{\omega_{s,\max}}{L}} \tag{17}$$

The integrand in equation (16) can be further simplified near RT when $\hbar\omega_{s,\max} > k_BT$, and it can be expressed as

$$F(\omega_{s,\min}) \approx -ln\{|exp(\hbar\omega_{s,\min}/k_BT) - 1|\} + \frac{\hbar\omega_{s,\min}}{k_BT} \frac{exp(\hbar\omega_{s,\min}/k_BT)}{exp(\hbar\omega_{s,\min}/k_BT) - 1} \tag{18}$$

Equations (17) and (18) constitute a simple analytical model for calculation of the thermal conductivity of graphene layer, which retains such important features of graphene phonon spectra as different υ_s and γ_s for *LA* and *TA* branches. The model also reflects the two-dimensional nature of heat transport in graphene all the way down to zero phonon frequency. Equation (18) reduces to Klemens' formula for graphene (26) in the limit $\xi \to 0$ ($\hbar\omega << k_BT$) and additional assumption of the same γ_s and υ_s for *LA* and *TA* phonons.

Using the equations summarized in the section IV we calculated the Umklapp-limited *intrinsic* thermal conductivity of graphene as a function of temperature. The results are shown in Figure 2 for several lateral sizes of graphene flakes. The Gruneisen parameters used in this calculation, $\gamma_{LA} = 1.8$ and $\gamma_{TA} = 0.75$, were obtained by averaging of $\gamma_s(q)$ (32). An experimental data point after Balandin et al. (3,4) is also shown for comparison. There is a good agreement between our model predictions and the available experimental data. One should note a very different temperature dependence obtained within this theoretical model for the relatively small (or narrow) graphene flakes (5 μm) as compared to that for large flakes (100 μm). In the very narrow graphene flakes and nanoribbons the thermal conductivity increases with temperature, which is related to the size (edge) effect on the phonon MFP.

Our model predictions are also in agreement with the tight-binding and non-equilibrium Green's function calculation of thermal transport in graphene nanoribbons reported in Ref. (8). Lan et al. (8) obtained a very strong width dependence of the thermal conductance for the narrow graphene ribbons with the width of about 2–20 carbon atoms. In their calculations the thermal conductance increases with the increasing width and with the temperature. This is similar to our results for the small (narrow) graphene flakes (see the curve for $L = 5$ μm in

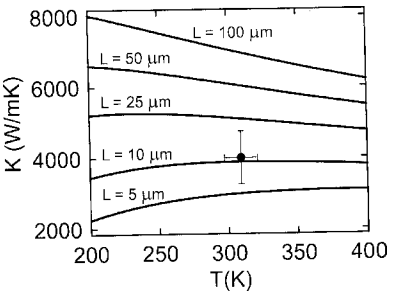

Figure 2. Theoretical thermal conductivity of graphene as a function of temperature. An experimental data point after Balandin et al. (3,4) is also shown for comparison.

Figure 2). The RT value of the thermal conductivity calculated by Lan et al. (8), K=3410 W/mK, is clearly above the bulk graphite limit of 2000 W/mK and in agreement with the experiments of Balandin et al. (3,4).

In Figure 3 we present the calculated RT thermal conductivity as a function of the flake lateral size. The dashed curves are obtained using equation (6) derived in section 3 with the total relaxation rate $1/\tau_{tot}(s,q) = 1/\tau^{K}_{U,s}(\omega_s(q)) + 1/\tau_B(s,q)$, explicitly taking into account the phonon scattering on graphene edges. The solid curve is obtained from equations (12–18) of the simplified approach outlined in the section IV in which the edge scattering is not directly included. Instead, the phonon MFP is limited by the physical size of the flake. The dashed curves are plotted for different values of the specularity parameter p. An experimental data point after Balandin et al. (3,4) is also shown for comparison. From both approaches we obtained similar dependences: the *intrinsic* thermal conductivity of graphene grows with the increasing linear size of the graphene flake. This is manifestation of the 2D-nature of the phonon transport in graphene.

Keep in mind that in the experimental conductions, the thermal conductivity will also be limited by extrinsic factors (e.g., defects, impurities, grain size), which prevent the growth of the thermal conductivity for very large flakes. With the decreasing specularity parameter p (more diffuse scattering) the thermal conductivity calculated with the boundary scattering term approaches the result obtained with the simple model. This is because in the simple

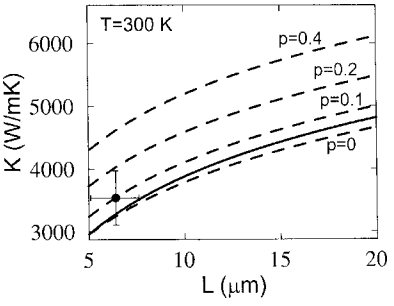

Figure 3. Theoretical thermal conductivity of graphene as a function of lateral dimensions of the layer. An experimental data point after Balandin et al. (3,4) is also shown for comparison.

model we neglect phonons with frequency $\omega < \omega_{\min,s}$ by completely restricting the phonon MFP to the lateral sizes of the flake. The latter corresponds to the perfectly diffusive scattering case (p=0). The described models are in good agreement with the measurements and shed light on the heat conduction properties of graphene.

Thermal Conduction in Carbon Allotropes and Derivatives

Carbon materials seem to occupy a somewhat unique place in terms of their ability to conduct heat: the values of thermal conductivity of different allotropes of carbon and their derivatives span a huge range from the lowest to the highest. Some forms of diamond-like carbons (DLC) have room-temperature thermal conductivity as low as 0.1 W/mK, amongst the lowest of any materials (33), while carbon nanotubes and graphene reveal thermal conductivities far exceeding 3000 W/mK, which are the highest values of all materials. Microcrystalline diamond (MCD), nanocrystalline diamond (NCD), ultra-nanocrystalline diamond (UNCD), tetrahedral amorphous carbon (ta-C) and carbon-based films occupy all range between these two extremes (33–36). Diamond, which is the best heat conductor among bulk materials, has the thermal conductivity values in the range from 800 W/mK to 2200 W/mK depending on the quality (37,38).

Table 1 summarizes the thermal conductivities of graphene, single-wallel carbon nanotubes (SWCNTs), multi-wallel carbon nanotubes (MWCNTs), and bulk carbon materials and thin films. The data on NCD, UNCD, ta-C and hydrogenated diamond-like carbon (DLCH) is based on the experimental results (33–36). The measurements were performed using a variety of techniques including the transient planar source (TPS) "hot-disk," 3-omega, and laser-flash techniques. The detailed analysis of the effects of the intrinsic atomic structure of carbon materials, example, sp^2 vs sp^3 bonding, cluster formation, etc., from the extrinsic, example, phonon scattering on interfaces, on the thermal conductivity of DLC, ta-C and NCD can be found in Refs. (33–36). From Table 1 one can also see that there is a wide data scatter for the reported values of the thermal conductivity of CNTs. The conventionally accepted values for CNTs are ~ 3000–3500 W/mK. Thus, graphene can outperform CNTs as the heat conductor. Owing to its planar geometry, graphene may have potential for lateral heat spreading. It still remains unclear though how the thermal

Table 1
Thermal conductivity of carbon materials

Sample	K (W/mK)	Method	Comments	Reference
graphene	~ 3080 – 5300	optical	single layer	Balandin et al. (3,4)
MW-CNT	> 3000	electrical	individual	Kim et al. (21)
SW-CNT	~ 3500	electrical	individual	Pop et al. (22)
SW-CNT	1750 – 5800	thermocouples	bundles	Hone et al. (23)
SW-CNT	> 3000	thermocouples	individual	Yu et al. (24)
graphite	~ 2000	variety	in-plane	Klemens (25,26)
DLCH	~ 0.6 – 0.7	3-omega	H: ~20–35%	Shamsa et al. (33)
NCD	~ 16	3-omega	grain size: 22 nm	Liu et al. (34)
UNCD	~ 6 – 17	3-omega	grain size: < 26 nm	Shamsa et al. (36)
ta-C	3.5	3-omega	sp^3: ~ 90%	Shamsa et al. (33)
ta-C	1.4	3-omega	sp^3: ~ 60%	Balandin et al. (35)
diamond	800 – 2000	laser flash	in-plane	Sukhadolau et al. (37)

conductivity of graphene will be affected when it is embedded inside a device structure or how the heat conduction ability will evolve with increasing the number of atomic layers. The theoretical models described in this review shed light on the differences in heat conduction in carbon materials. They can be incorporated into the simulation software for analysis of heat conduction in graphene layers and graphene devices (39,40). The superior thermal conductivity of graphene is beneficial for all of its proposed device applications, example, low-noise transistors, sensors, and interconnects (41,42).

Conclusions

We reviewed the results of our experimental and theoretical investigation of heat conduction in suspended graphene layers. We explained the enhanced thermal conductivity of graphene as compared to that of bulk graphite basal planes by the 2D nature of thermal transport in graphene over the whole range of phonon frequencies. The thermal conductivity in graphene was compared with that in other carbon materials. The superior thermal properties of graphene are beneficial for the proposed device applications.

We have recently reported the evolution of the thermal conductivity in few-layer graphene with addition of atomic layers (43). The intrinsic thermal conductivity of few-layer graphene approaches the bulk graphite limit as the number of atomic planes increases.

Acknowledgements

The work in Balandin Group was supported, in part, by DARPA – SRC through the FCRP Center on Functional Engineered Nano Architectonics (FENA) and Interconnect Focus Center (IFC). The authors are thankful to the current and former members of the Nano-Device Laboratory who contributed to this investigation. Special thanks go to Prof. C.N. Lau and her group members for the initial set of graphene samples made available for the study.

References

1. Novoselov, K. S., Geim, A. K., Morozov, S. V., Jiang, D., Zhang, Y., Dubonos, S. V., Grigorieva, I. V., and Firsov, A. A. (2004) Electric field effect in atomically thin carbon films. *Science*, 306:666–669; Novoselov, K. S., Geim, A. K., Morozov, S. V., Jiang, D., Katsnelson, M. I., Grigorieva, I. V., Dubonos, S. V., and Firsov, A. A. (2005) Two-dimensional gas of massless Dirac fermions in graphene. *Nature*, 438: 197–200.
2. Zhang, Y. B., Tan, Y. W., Stormer, H. L., and Kim, P. (2005) Experimental observation of the quantum Hall effect and Berry's phase in graphene. *Nature*, 438: 201–204.
3. Balandin, A. A., Ghosh, S., Bao, W., Calizo, I., Teweldebrhan, D., Miao, F., and Lau, C. N. (2008) Superior thermal conductivity of single-layer graphene. *Nano Letters*, 8: 902–907.
4. Ghosh, S., Calizo, I., Teweldebrhan, D., Pokatilov, E. P., Nika, D. L., Balandin, A. A., Bao, W., Miao, F. and Lau, C. N. (2008) Extremely high thermal conductivity of graphene: Prospects for thermal management applications in nanoelectronic circuits. *Appl. Phys. Lett.*, 92: 151911 (1–3).
5. Calizo, I., Miao, F., Bao, W., Lau, C. N., and Balandin, A. A. (2007) Variable temperature Raman microscopy as a nanometrology tool for graphene layers and graphene-based devices. *Appl. Phys. Lett.*, 91: 071913 (1–3).
6. Calizo, I., Balandin, A. A., Bao, W., Miao, F., and Lau, C. N. (2007) Temperature dependence of the Raman spectra of graphene and graphene multilayers. *Nano Letters*, 7: 2645–2649.
7. Nika, D. L., Pokatilov, E. P., Askerov, A. S., and Balandin, A. A. (2009) Phonon thermal conduction in graphene: Role of Umklapp and edge roughness scattering. *Phys. Rev. B.*, 79: 155413 (1–12).

8. Jiang, J. W., Wang, J. S., and Li, B. (2009) Thermal conductance of graphene and dimerite. *Phys. Rev. B.*, 79: 205418 (1–6).
9. Lan, J., Wang, J.-S., Gan, C. K., and Chin, S. K. (2009) Edge effects on quantum thermal transport in graphene nanoribbons: Tight-binding calculations. *Phys Rev B.*, 79: 115401 (1–5).
10. Ferrari, A. C., Meyer, J. C., Scardaci, V., Casiraghi, C., Lazzeri, M. Mauri, F., Piscanec, S., Jiang, D., Novoselov, K. S. Roth, S. and Geim, A. K. (2006) Raman spectrum of graphene and graphene layers. *Phys. Rev. Lett.*, 97: 187401 (1–4).
11. Calizo, I., Bao, W., Miao, F., Lau, C. N., and Balandin, A. A. (2007) The effect of substrates on the raman spectrum of graphene: Graphene-on-sapphire and graphene-on-glass. *Appl. Phys. Lett.*, 91: 201904 (1–3).
12. Calizo, I. Teweldebrhan, D., Bao, W., Miao, F., Lau, C. N., and Balandin, A. A. (2008) Spectroscopic raman nanometrology of graphene and graphene multilayers on arbitrary substrates. *J. Physics C*, 109: 012008 (1–4).
13. Parvizi, F., Teweldebrhan, D., Ghosh, S., Calizo, I. Balandin, A. A., Zhu, H, and Abbaschian, R. (2008) Properties of graphene produced by the high pressure-high temperature growth process. *Micro & Nano Letters*, 3: 29–34.
14. Dawlaty, J. M., Shivaraman, S., Chandrashekhar, M., Rana, F., and Spencer, M. G. (2008) Measurement of ultrafast carrier dynamics in epitaxial graphene. *Appl. Phys. Lett.*, 92: 042116 (1–3).
15. Sun, D., Wu, Z.-K., Berger, X., Divin, C., Li, C., de Heer, W. A. First, P. N., and Norris, T. B. (2008) Ultrafast relaxation of excited Dirac fermions in epitaxial graphene using optical differential transmission spectroscopy. *Phys. Rev. Lett.*, 10: 157402 (1–4).
16. Bolotin, K. I., Sikes, K. J., Hone, J., Stormer, H. L., and Kim, P. (2008) Temperature-dependent transport in suspended graphene. *Phys. Rev. Lett.*, 10: 096802 (1–4).
17. Krauss, B., Lohmann, T., Chae, D.-H., Haluska, M. Klitzing, K.-V., and Smet, J. H. (2009) Laser-induced disassembly of a graphene single crystal into a nanocrystalline network. *Phys. Rev. B*, 79: 165428 (1–9).
18. Nair, R. R., Blake, P., Grigorenko, A. N. Novoselov, K. S., Booth, T. J., Stauber, T., Peres, N. M. R., and Geim, A. K. (2008) Fine structure constant defines visual transparency of graphene. *Science*, 320: 1308.
19. Kim, K. S., Zhao, Y., Jang, H., Lee, S. Y., Kim, J. M., Kim, K. S., Ahn, J.-H., Kim, P., Choi, J.-Y., and Hong, B. H. (2009) Large-scale pattern growth of graphene films for stretchable transparent electrodes. *Nature*, 457: 706–710.
20. Mak, K. F., Sfeir, M. Y., Wu, Y., Lui, C. H., Misewich, J. A., and Heinz, T. F. (2008) Measurement of the optical conductivity of graphene. *Phys. Rev. Lett.*, 101: 196405 (1–4).
21. Kim, P., Shi, L. Majumdar, A., and McEuen, P. L. (2001) Thermal transport measurements of individual multi-walled nanotubes. *Phys. Rev. Lett.*, 87: 215502 (1–4).
22. Pop, E. Mann, D., Wang, Q., Goodson, K., and Dai, H. (2006) Thermal conductance of an individual single-wall carbon nanotube above room temperature. *Nano Letters*, 6: 96–100.
23. Hone, J., Whitney, M., Piskoti, C., and Zett, A. (1999) Thermal conductivity of single-walled carbon nanotubes. *Phys. Rev. B*, 59: R2514–R2516.
24. Yu, C. H., Shi, L., Yao, Z. Li, D. Y., and Majumdar, A. (2005) Thermal conductance and thermopower of an individual single-wall carbon nanotube. *Nano Letters*, 5: 1842–1846.
25. Klemens, P. G. (2000) Theory of the a-plane thermal conductivity of graphite. *J. Wide Bandgap Materials*, 7: 332–339.
26. Klemens, P. G. (2001) Theory of thermal conduction in thin ceramic films. *Int. J. Thermophysics*, 22: 265–275.
27. Srivastava, G. P. (1990) *The Physics of Phonons*, IOP: Philadelphia, PA, p. 99; Bhandari, C. M. and Rowe, D. M. (1988) *Thermal Conduction in Semiconductors*, Wiley: New York.
28. Klemens, P. G. (1958) *Solid State Physics*, Seitz, F. and Turnbull, D., Academic: New York vol. 7, p. 1.
29. Han, Y.-J. and Klemens, P. G. (1993) Anharmonic thermal resistivity of dielectric crystals at low temperatures. *Phys. Rev. B*, 48: 6033–6042.
30. Ziman, J. M. (2001) *Electrons and Phonons*, Clarendon Press: Oxford, UK, p. 463.

31. Mounet, N. and Marzari, N. (2005) First-principles determination of the structural, vibrational and thermodynamic properties of diamond, graphite, and derivatives. *Phys. Rev. B*, 71: 205214 (1–14).
32. Nika, D. L., Ghosh, S., Pokatilov, E. P., Balandin, A. A. (2009) Lattice thermal conductivity of graphene flakes: Comparison with bulk graphite. *Appl. Phys. Lett.*, 94: 203103 (1–3).
33. Shamsa, M., Liu, W. L., Balandin, A. A., Casiraghi, C., Milne, W. I., and Ferrari, A. C. (2006) Thermal conductivity of diamond-like carbon films. *Appl. Phys. Lett.*, 89: 161921 (1–3).
34. Liu, W. L., Shamsa, M., Calizo, I. Balandin, A. A., Ralchenko, V., Popovich, A., and Saveliev, A., Thermal conduction in nanocrystalline diamond films: Effects of the grain boundary scattering and nitrogen doping. *Appl. Phys. Lett.*, 89: 171915 (1–3).
35. Balandin, A. A., Shamsa, M., Liu, W. L., Casiraghi, C., and Ferrari, A. C. (2008) Thermal conductivity of ultrathin tetrahedral amorphous carbon films. *Appl. Phys. Lett.*, 93: 043115 (1–3).
36. Shamsa, M. Ghosh, S., Calizo, I. Ralchenko, V., Popovich, A., and Balandin, A. A. (2008) Thermal conductivity of nitrogenated ultrananocrystalline diamond films on silicon. *J. Appl. Phys.*, 103: 083538 (1–8).
37. Sukhadolau, A. V., Ivakin, E. V., Ralchenko, V. G., Khomich, A. V., Vlasov, A. V., Popovich, A. F. (2005) Thermal conductivity of CVD diamond at elevated temperatures. *Diamond Relat. Mater.*, 14: 589–593.
38. Worner, E., Wild, C., Muller-Sebert, W., Locher, R., and Koidl, P. (1996) Thermal conductivity of CVD diamond films: High-precision, temperature-resolved measurements. *Diamond Relat. Mater.*, 5: 688–692.
39. Subrina, S. and Kotchetkov, D. (2008) Simulation of heat conduction in suspended graphene flakes of variable shapes. *J. Nanoelectronics and Optoelectronics*, 3: 249–269.
40. Ko, G. and Kim, J. (2009) Thermal modeling of graphene layer on the peak channel temperature of AlGaN/GaN high electron mobility transistors. *Electrochemical and Solid-State Letters*, 12: H29–H31.
41. Shao, Q., Liu, G., Teweldebrhan, D., Balandin, A. A., Rumyantsev, S., Shur, M., and Yan, D. (2009) Flicker noise in bilayer graphene transistors. *IEEE Electron Device Letters*, 30: 288–290.
42. Shao, Q., Liu, G., Teweldebrhan, D., and Balandin, A. A. (2008) High-temperature quenching of electrical resistance in graphene interconnects. *Appl. Phys. Lett.*, 92: 202108 (1–3).
43. Ghosh, S., Bao, W., Nika, D. L., Subrina, S., Pokatilov, E. P., Lau, C. N., and Balandin, A. A. (2010) Dimensional crossover of thermal transport in few-layer graphene. *Nature Materials*, 9: 555.